ChemPubSoc Europe

DOI: 10.1002/cbic.201500619

CHEMBIOCHEM Full Papers

VIP *Very Important Paper*

SPECIAL ISSUE

Solution Observation of Dimerization and Helix Handedness Induction in a Human Carbonic Anhydrase–Helical Aromatic Amide Foldamer Complex

Michal Jewginski,[b, c] Lucile Fischer,[b] Cinzia Colombo,[b] Ivan Huc,*[b] and Cameron D. Mackereth*[a]

In memory of Dr. Bernard Gallois

The design of synthetic foldamers to selectively bind proteins is currently hindered by the limited availability of molecular data to establish key features of recognition. Previous work has described dimerization of human carbonic anhydrase II (HCA) through self-association of a quinoline oligoamide helical foldamer attached to a tightly binding HCA ligand. A crystal structure of the complex provided atomic details to explain the observed induction of single foldamer helix handedness and revealed an unexpected foldamer-mediated dimerization. Here, we investigated the detailed behavior of the HCA–foldamer complex in solution by using NMR spectroscopy. We found that the ability to dimerize is buffer-dependent and uses partially distinct intermolecular contacts. The use of a foldamer variant incapable of self-association confirmed the ability to induce helix handedness separately from dimer formation and provided insight into the dynamics of enantiomeric selection.

Introduction

Synthetic foldamers have undergone rapid development, driven mainly by curiosity and by the hope that foldamers could achieve functions that match or even go beyond those of biopolymers.[1] This progress has led to the finding of varied artificial molecular backbones that adopt well-defined folded conformations. Among these, aromatic amide foldamers[2] stand out owing to the following features: exceptionally predictable, tunable, and stable conformations in solution; relatively easy synthesis of sequences bearing various proteinogenic side chains, including on solid support;[3] accessibility of secondary and tertiary-like objects as large as small proteins;[4] and a high amenability to crystal growth and accurate structural elucidation. Appending polar side chains endows these aromatic backbones with solubility in protic medium,[5] in which their conformational stability may be enhanced by intramolecular hydrophobic effects.[6] These features all point to aromatic amide foldamers as potential scaffolds to construct ligands for large protein surface areas and possible inhibitors of protein–protein interactions or protein–nucleic acid interactions. Because of the very nature of aromatic backbones, these would fundamentally differ from peptidic foldamers that may also recognize protein surfaces.[7] As pioneering examples, a number of rigid rods have been developed that are composed of aromatic amides, ureas, or oligoaryl derivatives. For example, aromatic α-helix mimetics may inhibit some protein–protein interactions,[5a,8] with certain anionic sequences shown to interact with the 37-residue islet amyloid polypeptide (IAPP).[9] Pyrrole–imidazole oligoamides have long been known to bind the minor groove of double-stranded DNA,[10] and helical cationic sequences specifically recognize G-quadruplex DNA.[11]

In the development of an aromatic oligoamide specific for a particular target, obtaining high-resolution structural information on foldamer–target interactions will yield important advantages for iteratively improving binding affinity and selectivity. A recent example of such structure-based iterative sequence evolution yielded a foldamer that tightly and selectively recognized β-fructopyranose.[12] In a different context, the structural characterization of anti-parallel stacked oligo-pyrrole–imidazole dimers in the minor groove of B-DNA was also essential for their development.[13] However, in the absence of

[a] *Dr. C. D. Mackereth*
University of Bordeaux, ARNA (U1212)
Institut Européen de Chimie et Biologie
and
INSERM, ARNA (U1212)
and
CNRS, ARNA (UMR 5320)
2 rue Escarpit, 33600 Pessac (France)
E-mail: c.mackereth@iecb.u-bordeaux.fr

[b] *Dr. M. Jewginski, Dr. L. Fischer, Dr. C. Colombo, Dr. I. Huc*
University of Bordeaux, CBMN (UMR 5248)
Institut Européen de Chimie et Biologie
2 rue Escarpit, 33600 Pessac (France)
and
CNRS, CBMN (UMR 5248)
and
Bordeaux Institut National Polytechnique, CBMN (UMR 5248)
E-mail: i.huc@iecb.u-bordeaux.fr

[c] *Dr. M. Jewginski*
Wrocław University of Technology
Faculty of Chemistry, Wrocław (Poland)

Supporting information and the ORCID identification number(s) for the author(s) of this article can be found under http://dx.doi.org/10.1002/cbic.201500619.This manuscript is part of a joint Special Issue between ChemBioChem *and* ChemMedChem *on Protein–Protein Interactions.*

sufficient starting affinity, that is, in the context of ab initio design, obtaining structural information is not possible, reducing the hope to improve binding. To overcome this obstacle, we surmised that tethering a foldamer to a protein surface might allow the detection and understanding of even weak interactions and provide a starting point for iterative improvements.

We previously used human carbonic anhydrase II (HCA) as a model system because this protein is known to crystallize easily—the Protein Data Bank contains over 500 crystal structures—and because synthetically accessible nanomolar ligands derived from aromatic sulfonamides exist that can be appended to a foldamer and ensure a non-covalent yet tight linkage to HCA. In a recent report,[14] we described the synthesis of short helical foldamers based on quinolinecarboxamides, each having an appended HCA ligand.[15] The foldamers did not contain any stereogenic center and initially existed as racemic mixtures of right- (*P*) or left-handed (*M*) helices. However, when the foldamers were confined to the HCA surface through binding of the ligands to the HCA active site, interactions were detected by circular dichroism (CD), which revealed a helix handedness bias for some foldamers, induced by preferential interactions of either the *P* or *M* helix with the inherently chiral protein surface.[14,16,17] By using this method, compound **1** (Figure 1) was identified as having a strong preference for *P*-handedness when linked to HCA.

The HCA–**1** complex was successfully crystallized, and its structure in the solid state was solved.[14] The structure revealed a dimerization process through which two foldamers and two HCA molecules assemble into a larger (HCA–**1**)$_2$ structure, stabilized by 1) a number of foldamer–protein interactions, including a Zn^{2+} bridging complex; 2) foldamer–foldamer hydrophobic contacts; and 3) new HCA-HCA interactions. The structure also confirmed the *P* helicity of the bound foldamer. This foldamer-mediated dimerization of HCA somewhat relates to the dimerization of other proteins, achieved by appending a peptide known to dimerize,[18] or through the use of ditopic protein ligands.[19] The dimerization process and the foldamer–HCA interactions, as revealed by the crystal structure, could not otherwise have been predicted, highlighting the potential of the tethering approach. The solid-state structure constitutes the basis of further design and improvements which are in progress and will be reported in due time.

The prime objectives of the present study are to assess whether the unanticipated foldamer-mediated dimerization of HCA observed in the solid state also occurs in solution and to gain insights into the solution structure of the complex. The (HCA-**1**)$_2$ crystals were grown in an extremely zinc-rich medium (100 mM zinc acetate), leading to abundant Zn^{2+} in the crystal structure, including at places that suggest a possible contribution to dimerization (foldamer–protein contacts and protein–protein contacts within the dimer). In contrast, the initial CD screening in solution revealed that the preferred *P* helicity of the HCA–**1** complex was present without any added Zn^{2+}. We now report that **1** does mediate HCA dimerization in solution in the absence of added Zn^{2+} and that this process is buffer-dependent and also selective for the sequence of **1**. Nevertheless, the (HCA-**1**)$_2$ dimer formed in the absence of Zn^{2+} in solution is structurally less well defined. We also report that handedness induction does not require dimerization; thus, foldamer–protein interactions other than those observed in the solid state exist in 1:1 HCA–**1** complexes. These solution studies provide important insight into the behavior and molecular details of foldamer–protein interactions in solution.

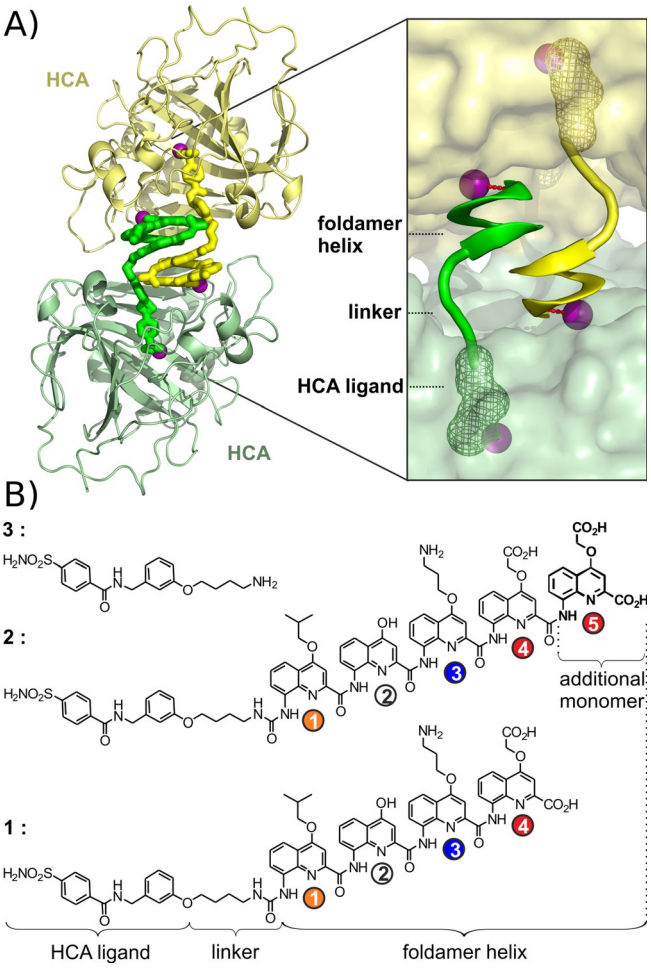

Figure 1. Foldamers and HCA–foldamer complex. A) Crystal structure (left) of the (HCA–**1**)$_2$ dimer,[14] and schematic view (right) of the foldamer–protein interface. Proteins are represented as ribbons (left) or as solvent-accessible surfaces (right). Foldamers are shown in the same color (green or yellow) as the color to which their ligand moiety is attached. Zinc ions at the bottom of the ligand binding pocket and at the foldamer–protein interface are shown as purple spheres. B) Formulae of compounds **1**–**3**.

Results and Discussion

NMR spectroscopy of protein–foldamer interactions

In order to characterize the behavior of HCA–**1** in solution, we first pursued a biophysical approach by using NMR spectroscopy to provide protein residue-specific information on intermolecular HCA–foldamer and HCA–HCA interactions.[20] For this purpose, we prepared samples of ^{13}C,^{15}N-isotopically enriched HCA ([^{13}C,^{15}N]HCA) in two biological buffers and assigned the protein backbone ^{1}H, ^{13}C, and ^{15}N chemical shifts based on pre-

viously reported values.[21] Well-resolved 2D $^{1}H,^{15}N$ TROSY and $^{1}H,^{15}N$ HSQC spectra, combined with nearly complete amide annotation, demonstrated that HCA in buffered solutions containing 50 mM Tris (2-amino-2-hydroxymethyl-propane-1,3-diol) pH 8.0 or 50 mM sodium phosphate pH 7.4 (Figure S1) were equally suitable for detailed analysis by NMR spectroscopy.

The $^{1}H,^{15}N$ chemical shift values of protein backbone amides are exquisitely sensitive to changes in their local environment[22] and thus serve as simple but informative reporters for protein regions involved in ligand binding. We therefore added the modified aromatic sulfonamide inhibitor **3** to ^{15}N-labeled HCA and observed the resulting $^{1}H,^{15}N$ amide chemical shift perturbation of [^{15}N]HCA in Tris and phosphate buffers (Figure S2). Using the titration in Tris as an example, the addition of saturating amounts (1.3 molar equivalents) of **3** resulted in significant perturbation of a number of amide crosspeaks (selected region shown in Figure 2A). Calculation of the combined $^{1}H,^{15}N$ perturbation ($\Delta\delta_{H,N}$) revealed residues most affected by the inhibitor (Figure 2B), which we have classified as amides with no apparent movement (<0.25 ppm) as well as residues with increasing perturbation.

The $\Delta\delta_{H,N}$ values were mapped onto the three-dimensional structure of HCA, with each measured amide crosspeak shown as a sphere (Figure 2C) using the color gradient from Figure 2B. Residues with $\Delta\delta_{H,N}$ greater than 0.25 ppm precisely mapped to the central cavity region of HCA. This region, identified in solution to be in close proximity to bound inhibitor **3**, reassuringly coincided with backbone amides located within 6 Å of the inhibitor within the crystal structure of (HCA–**1**)$_2$ (circled regions in Figure 2C and D). Measurements in phosphate buffer revealed the same pattern of residues affected by inhibitor binding (Figure S3A–C).

The next step was to determine which residues were adjacent to the foldamer moiety when appended to the HCA ligand. In the crystal structure, the quinoline oligoamide portion of compound **1** is involved in dimerization; thus, we would expect significant $\Delta\delta_{H,N}$ values for residues in contact with either of the two quinoline moieties in the dimer complex, as well as residues contacting the second HCA protein. A saturating amount of compound **1** was therefore added to [^{15}N]HCA, and calculation of $\Delta\delta_{H,N}$ was used to identify residues that experience a change in chemical environment induced by **1**. In this case, the spectrum of HCA–**1** was compared with HCA–**3** in order to eliminate the contribution of the inhibitor and obtain information only on those peaks affected by the foldamer itself (Figure S4). Importantly, these experiments were carried out in the absence of any added Zn^{2+}. Indeed, addition of a molar equivalent of Zn^{2+} induced significant precipitation, preventing detailed study by NMR spectroscopy

Again using Tris buffer samples as an example, several amide crosspeaks were shifted when comparing the $^{1}H,^{15}N$ TROSY spectra of HCA–**1** with HCA–**3** (Figure 2E and F). When mapped to the structure of HCA, perturbation specific to the addition of the foldamer primarily was observed around one side of the entrance to the inhibitor-binding cavity (Figure 2G). In the previous crystal structure, several amides were within 6 Å of either of the two bound quinoline oligoamide

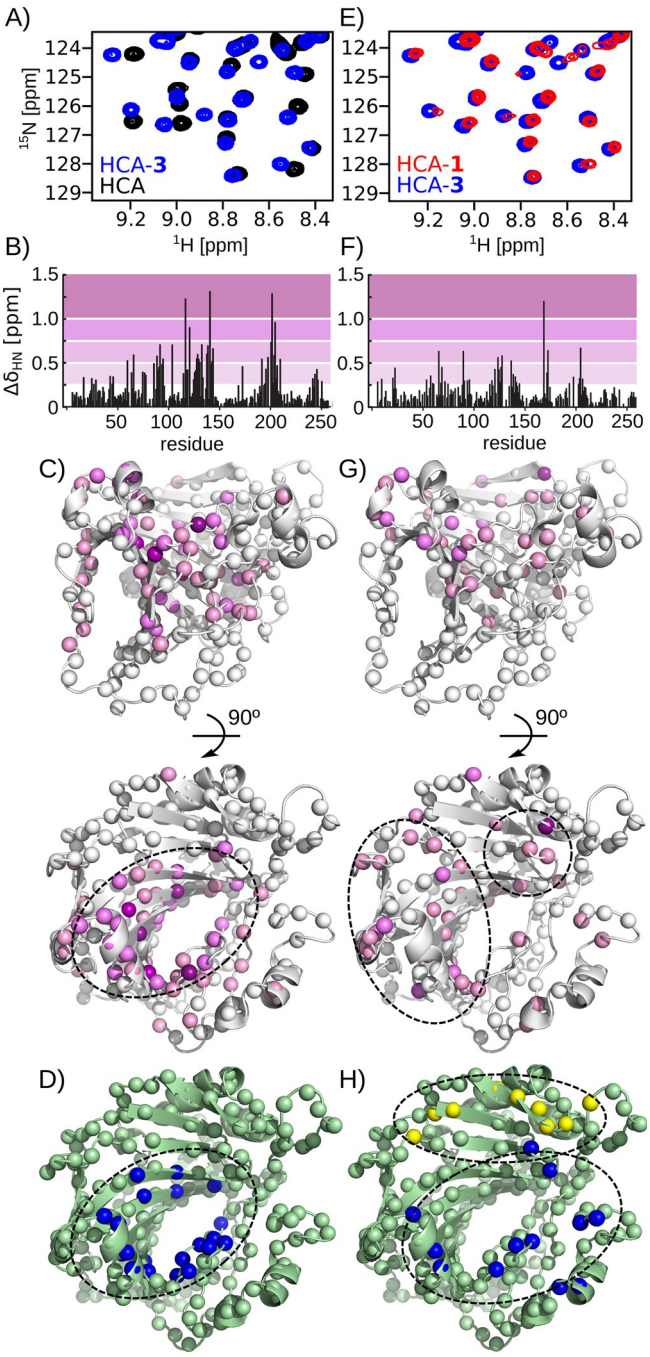

Figure 2. Intermolecular contacts identified by NMR spectroscopy in Tris buffer. A) Region of $^{1}H,^{15}N$ TROSY spectra (Figure S2A) from samples of unbound 300 μM [^{15}N]HCA without (black) and with (blue) 1.3 molar equivalents of compound **3** added. B) $\Delta\delta_{H,N}$ of HCA–**3** compared to HCA, calculated as the root mean square deviation, $((\Delta\delta_H/0.14)^2+(\Delta\delta_N)^2)^{0.5}$.[22] C) Each observed amide nitrogen atom in the $^{1}H,^{15}N$ TROSY is represented as a sphere on the structure of HCA (chain A from PDB ID: 4LP6)[14] and colored as in (B). The top orientation is the same as for the green HCA protein in Figure 1A. D) Amide nitrogen atoms (spheres) of residues located less than 6 Å from the sulfonamide inhibitor atoms within the crystal structure. E) Region of $^{1}H,^{15}N$ TROSY spectra (Figure S4A) of HCA–**1** (red) and HCA–**3** (blue) in Tris buffer. F) $\Delta\delta_{H,N}$ of HCA–**1** compared to HCA–**3**, calculated as in (B). G) Each observed amide is represented as a sphere on the structure of HCA and colored as in (F). H) Amide nitrogens (spheres) of residues located within 6 Å of the foldamer moieties of compound **1** in the HCA–**1** complex structure (blue) or along the HCA–HCA dimer interface (yellow).

moieties (blue spheres, Figure 2H) or along the newly formed HCA–HCA dimer interface (yellow spheres, Figure 2H). In contrast to the previous analysis with compound **3**, there was only partial overlap between the binding region identified in solution and the intermolecular contacts in the crystal structure of $(HCA–\mathbf{1})_2$. Instead, the contact region identified by NMR spectroscopy (circled in Figure 2G) appeared to mainly occupy an area between the crystal structure contact regions (circles in Figure 2H). This discrepancy was also observed in the comparison of HCA–**1** with HCA–**3** in phosphate buffer (Figure S3D–F). In this latter buffer, however, we clearly noted line-broadening in the $^{1}H,^{15}N$ HSQC spectrum of HCA–**1** that could be indicative of a significant increase in molecular size. This latter finding supports a shared ability of compound **1** to induce dimerization both in solution and in the crystal, despite the otherwise different surfaces involved in intermolecular contacts. To better analyze the oligomerization state of HCA under various conditions, we used NMR spectroscopy methods sensitive to the overall molecular size.

HCA–1 dimerization in solution

The rotational correlation time (τ_c) of a protein or protein complex is a function of the hydrodynamic radius and is therefore related to the molecular size and shape. Higher oligomeric species of a protein are reflected by a predictable increase in the value of τ_c. One method to measure protein τ_c and to address the oligomeric state of HCA–**1** in solution, is by the combined determination of the backbone amide ^{15}N longitudinal (T_1) and transverse (T_2) relaxation rates for a ^{15}N-labeled protein sample.[23] Starting with the unbound [^{15}N]HCA at 295 K and a field strength of 700 MHz, we determined residue-specific values for T_1 and T_2 in phosphate buffer (Figure 3A and B). These values are in excellent agreement with T_1 and T_2 values of monomeric HCA, as predicted using the program HYDRONMR[24] (grey circles in Figure 3A and B), based on the atomic structure of HCA (PDB ID: 4CAC).[25] Measurement of heteronuclear {^{1}H}^{15}N NOE values greater than 0.6 (Figure 3C) indicated that most observable backbone amides were conformationally rigid with respect to the HCA molecule. The measured T_1 and T_2 values of these rigid amides thus primarily relate to the overall motion of the protein instead of localized dynamics. Based on the T_1:T_2 ratio of these residues, we obtained a τ_c value of 16.4 ns for HCA using TENSOR version 2.0.[26] This experimental value correlated extremely well with the prediction from HYDRONMR (16.4 ns). We next attempted to obtain ^{15}N relaxation measurements of [^{15}N]HCA–**1**. Unfortunately, the significant line-broadening in the required 2D spectra precluded a similar residue-based analysis. As a result, we elected to perform a simplified estimate of correlation time based only on 1D ^{1}H NMR spectra.

In this simplified approach to determine τ_c, a series of 1D ^{1}H NMR spectra were collected to correlate signal reduction of the backbone amide $^{1}H^{N}$ with increasing relaxation delays.[27] Although the accuracy is diminished as compared to ^{15}N-based determination of τ_c, this method is rapid, suitable for large proteins, and ^{15}N-labeling is not required. We collected spectra on

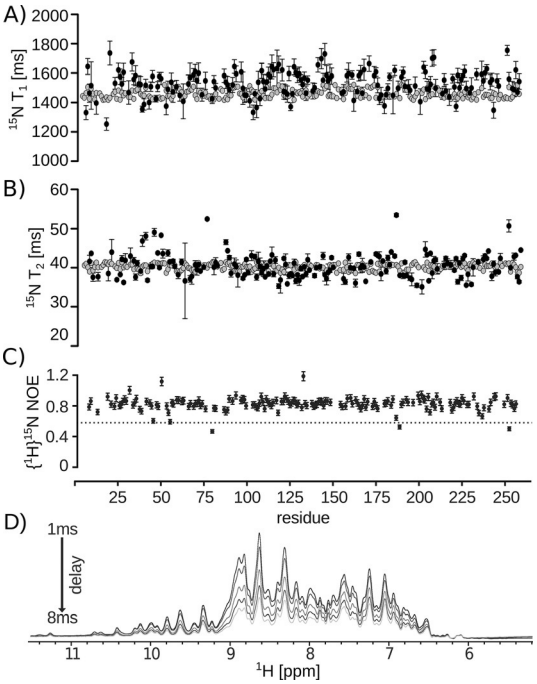

Figure 3. Correlation time determination of HCA in phosphate buffer. Residue-specific measurement of the ^{15}N relaxation parameters A) T_1 and B) T_2 and C) the heteronuclear {^{1}H}^{15}N NOE on a sample of 500 μM [^{15}N]HCA in phosphate buffer at 295 K. Gray circles are the predicted values of ^{15}N T_1 and T_2 by using HYDRONMR[24] with the monomeric structure of HCA (PDB ID: 4CAC).[25] D) Approximation of τ_c on the same phosphate sample of 500 μM ^{15}N-HCA by using a 1D ^{1}H NMR series with increasing relaxation delays of 1, 2, 4, 6, and 8 ms (Table 1).

the same phosphate sample of 500 μM HCA as in Figure 3A, with delays of 1, 2, 4, 6, and 8 ms (Figure 3D). The spectra and delays were converted to a $^{1}H^{N}$ amide T_2 value of 13.7 ± 0.6 ms (Table 1).[28] As an accurate τ_c value for this sample was determined by ^{15}N relaxation to be 16.4 ns (data in Figure 3), we were able to establish a specific conversion equation of $\tau_c = (4.45 \cdot T_2)^{-1}$. The next step was to look at a sample of 500 μM HCA–**1** in the same buffer and at the same temperature and field strength. The observed $^{1}H^{N}$ amide T_2 value of 7.8 ± 0.5 ms corresponds to a τ_c of 28.8 ns. This approximate doubling of

Table 1. Molecular size of HCA, HCA–**1**, and HCA–**2** in solution by using 1D $^{1}H^{N}$ NMR T_2 relaxation measurements to estimate the correlation time.

Sample	Conc. [μM]	Buffer[a]	$^{1}H^{N}$ T_2 [ms]	τ_c [ns][b]
HCA	500	phosphate	13.7 ± 0.6	16.4
HCA–**1**	500	phosphate	7.8 ± 0.5	28.8
HCA	70	phosphate	14.5 ± 0.9	15.5
HCA–**1**	70	phosphate	7.4 ± 0.8	30.4
HCA	300	Tris	13.8 ± 1.1	16.2
HCA–**1**	300	Tris	11.0 ± 0.6	20.4
HCA–**1**	200	Tris	11.5 ± 0.7	19.5
HCA–**1**	100	Tris	12.7 ± 0.7	17.7
HCA–**2**	500	phosphate	12.1 ± 0.6	18.6
HCA–**2**	300	Tris	12.2 ± 1.4	18.4

[a] Phosphate, 50 mM sodium phosphate (pH 7.4); Tris, 50 mM Tris (pH 8.0). [b] Estimate of correlation time (τ_c) by using the equation $\tau_c = (4.45 \cdot T_2)^{-1}$.

the correlation time is fully consistent with the formation of a dimer and supports the presence in solution of the (HCA–**1**)$_2$ found in the crystal structure. We next repeated the analysis with diluted samples of 70 μM HCA and HCA–**1**, with no significant changes in τ_c values (15.5 ns and 30.4 ns, respectively, Table 1). The results indicate that, in phosphate buffer, the HCA monomer and HCA–**1** dimer is maintained within a seven-fold protein concentration range and that dissociation of HCA–**1** might only occur at lower concentrations.

We then analyzed samples in Tris buffer, starting with a sample of 300 μM HCA. Again, a clear protein monomeric state was observed, as evidenced by a $^1H^N$ amide T_2 value of 13.8 ± 1.1 ms and a τ_c value of 16.2 ns (Table 1). When we analyzed the effect of compound **1**, only a 50% increase in τ_c was detected over unbound HCA (20.4 ns compared to 16.2 ns). This finding is in contrast to the clear dimer formed in phosphate buffer, possibly due to a shift in equilibrium towards monomeric HCA–**1**. Serial dilution of HCA–**1** to 200 and 100 μM was accompanied by a steady decrease in τ_c (19.5 and 17.7 ns, respectively) towards the value observed for the HCA monomer. The association of the HCA–**1** dimer in Tris is therefore weaker than in phosphate, implying a buffer-dependent effect on HCA–**1** dimerization. To further investigate the process of dimer formation, a modification of compound **1** was sought that could not self-associate.

By using the crystal structure to suggest changes to the foldamer that could disrupt the ability to dimerize, we designed and synthesized compound **2** (Figure 1B). The modification involves an extension of the foldamer terminus by adding one extra quinoline bearing an acidic side chain. There is insufficient free space in the (HCA–**1**)$_2$ structure to accommodate the added quinoline without having the extension protrude into the HCA protein. It was therefore predicted that this small addition would be enough to prevent dimerization of HCA–**2**. Elongation to a sequence comprised of more than five quinoline units was not considered, as longer helices require excessive amounts of time to shift the equilibrium between right-handed and left-handed helices, particularly in water,[6,29] preventing the ability to measure handedness induction in later experiments.

Consistent with the predicted ability to disrupt dimerization, $^1H^N$ T_2 relaxation measurements on samples of HCA–**2** demonstrated a size reduction in both phosphate and Tris buffers (Table 1). In addition, detailed analysis of backbone amide ^{15}N T_2 relaxation of [^{15}N]HCA–**2** in phosphate at 295 K and a field strength of 700 MHz (Figure 4A) yielded average rates that were comparable to the unbound [^{15}N]HCA (Figure 3B). Finally, we tested the oligomerization state of HCA–**2** by using size-exclusion chromatography (Figure 4B). Samples of 500 μM HCA, HCA–**1**, and HCA–**2** in phosphate buffer were analyzed by using a Superdex 75 size-exclusion chromatography column. Both HCA and HCA–**2** eluted at a similar volume, whereas HCA–**1** eluted at an earlier volume, consistent with the larger molecular size of the dimer. Taking advantage of HCA–**2** as a confirmed monomer, we were able to investigate whether dimerization is a requirement for helix handedness induction.

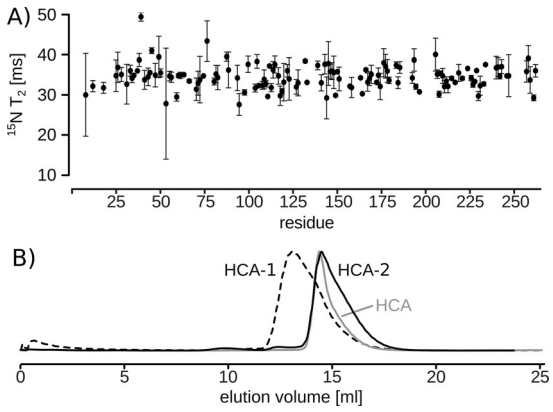

Figure 4. Monomeric state of HCA–**2**. A) Residue-specific determination of ^{15}N T_2 relaxation on a sample of 500 μM [^{15}N]HCA–**2** in phosphate buffer at 295 K. B) Analysis of HCA (——), HCA–**1** (- - - -), and HCA–**2** (——) by size-exclusion chromatography. The vertical axis is absorption at 280 nm, normalized to the maximum value.

Induction of foldamer right-handedness by the protein surface

The results in Table 1 and Figure 4B indicate the dimerization of HCA–**1** at micromolar concentrations in the same medium (phosphate buffer without Zn^{2+}), in which induced CD was observed in the original characterization of HCA–**1**.[14] This preferred right-handedness was confirmed in the crystal structure of (HCA–**1**)$_2$. Several questions then arose: is handedness induction in HCA–**1** reliant on dimerization of the complex? In other words, were we observing the dimerization of HCA–**1** complexes in which **1** was already *P*-helical, or were we observing dimerization-promoted handedness induction of **1**? And what is the behavior of the monomeric **2** bound to HCA?

We began to address these questions using CD spectroscopy to determine if compound **2** within the monomeric HCA–**2** complex was also shifted towards a single enantiomer. CD spectra of 34 μM HCA–**2** in Tris or phosphate both indicated a surprisingly strong induction of a *P* helix (Figure 5A), similar to that of (HCA–**1**)$_2$. Furthermore, the molar circular dichroism ($\Delta\varepsilon^{390}$) per residue of HCA–**2** was 12.4 L mol^{-1} cm^{-1} res^{-1} (Tris) and 12.7 L mol^{-1} cm^{-1} res^{-1} (phosphate), which was comparable to the previously reported value of 11.5 L mol^{-1} cm^{-1} res^{-1} for 34.5 μM HCA–**1** in phosphate.[14] The molar circular dichroism per residue for HCA–**2** does not depend on concentration, as measurements at 6.8 and 200 μM have comparable values (Figure 5A). As HCA–**2** is a monomer, this suggests that dimerization is not a required factor in handedness induction of compound **2**. Instead, induction must be due to direct interaction between the foldamer moiety and the surface of HCA. If this is the case for **2**, then it is possible that compound **1** is also already in a preferred enantiomeric state, independent of HCA–**1** dimer formation.

Results in Table 1 revealed that dimerization of HCA–**1** in Tris buffer was strongly diminished. Nevertheless, measurement of CD spectra in samples of HCA–**1** at 200, 34, and 6.8 μM showed induced CD bands indicative of a preferred right-handedness (Figure 5B). The results indicate that, even under condi-

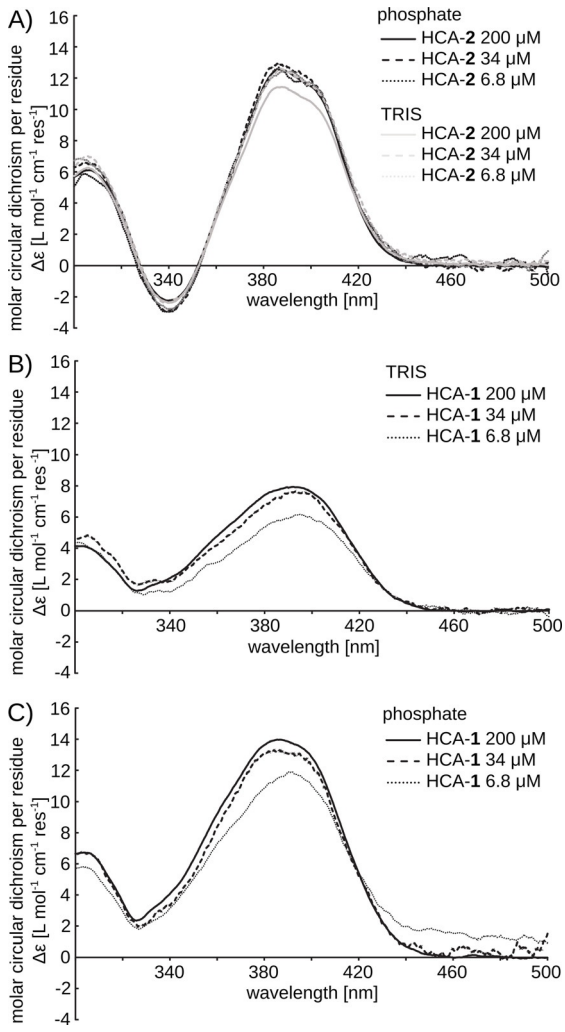

Figure 5. CD spectra of HCA–**2** and HCA–**1** complexes in aqueous phosphate and Tris buffers. A) Molar circular dichroism per residue at 293 K for three concentrations of HCA–**2** in both phosphate and Tris. CD curves of HCA–**2** in phosphate at 200 μM (——), 34 μM (-----), and 6.8 μM (····). CD curves of HCA–**2** in Tris at 200 μM (——), 34 μM (-----), and 6.8 μM (····). B) Molar circular dichroism per residue of HCA–**1** in Tris at concentrations of 200 μM (——), 34 μM (-----), and 6.8 μM (····). C) Molar circular dichroism per residue of HCA–**1** in phosphate at concentrations of 200 μM (——), 34 μM (-----), and 6.8 μM (····).

tions in which HCA–**1** was essentially monomeric (i.e., 6.8 μM), handedness induction was still effective. Dimer formation of (HCA–*P*-**1**)$_2$ was therefore the result of the dimerization of HCA–*P*-**1** and not the *P*-handedness induction of HCA–racemic-**1** upon dimerization. This indicates pre-existing diastereoselective interactions between HCA and **1** in HCA–*P*-**1** that are not seen in the crystal structure of (HCA–*P*-**1**)$_2$, in which each foldamer interacts with the protein surface to which the other foldamer is bound. However, we noted that the $\Delta\varepsilon^{390}$ values in Tris of 7.9, 7.5, and 5.9 L mol^{-1} cm^{-1} res^{-1} for 200, 34, and 6.8 μM HCA–**1**, respectively, were smaller than the corresponding measurements in phosphate (Figure 5C). This suggests that enhanced dimerization in phosphate buffer might act to further stabilize the pre-existing enantiomer preference. In order to shed light on the underlying protein–foldamer interactions that give rise to helix handedness, we then focused our attention onto the characterization of HCA–*P*-**2**.

Foldamer–protein interactions in HCA–2

To gain insight into enantiomer selection for HCA–*P*-**2**, we collected ^{1}H,^{15}N TROSY and HSQC spectra on the [^{15}N]HCA–**2** complex in Tris and phosphate buffers, respectively (Figure S5). Due to a number of chemical shift changes in keeping with an efficient formation of the HCA–**2** complex (Figure 6A), we first confirmed the identity of the crosspeaks by using 3D HNCA and HNCO spectra. Similar to the analysis of HCA–**1**, we calculated $\Delta\delta_{H,N}$ values compared to the chemical shift values of the inhibitor-bound HCA–**3** (Figure 6B). There was a prominent

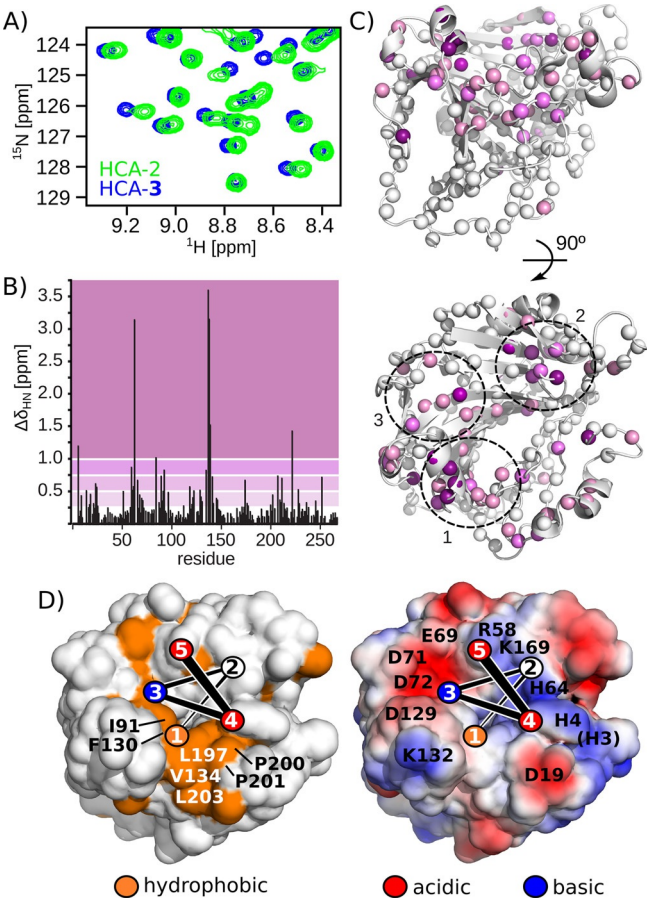

Figure 6. Intermolecular contacts within HCA–**2**. A) Selected region of the superimposition of ^{1}H,^{15}N TROSY spectra of HCA–**2** (green) and HCA–**3** (blue) in Tris buffer (Figure S6A). B) $\Delta\delta_{H,N}$ of HCA–**2** compared to HCA–**3**, calculated as in Figure 2B. C) Each observed amide is represented as a sphere on the structure of HCA (chain A from PDB ID: 4LP6)[14] and colored as in (B). The circles highlight clusters of amides with significant chemical shift perturbations. D) Surface representations of HCA in the same orientation as the bottom image of (C). Hydrophobic side chains are colored orange and are annotated with residue type and number (left). A model of compound **2** is placed on the surface of HCA, illustrating the putative position of the five quinoline monomers (see Figure 1B for the atomic structure of compound **2**). Surface representation colored by calculated charge (PyMOL Molecular Graphics System, version 1.7.4, Schrödinger) is shown at right, with acidic regions in red and basic regions in blue. Selected charged residues are annotated with residue type and number.

grouping of the amides experiencing chemical shift perturbation by the foldamer moiety of compound **2**, and three major clusters were identified (circles 1, 2, and 3 in Figure 6C).

From CD spectroscopy, we know that compound **2** favors a right-handed helix within the monomeric HCA–**2** (Figure 5A). Inspection of the surface properties of HCA can provide insight into the origin of the main regions of chemical shift perturbation. The first cluster of perturbed amides (circle 1 in Figure 6C) co-localized with a hydrophobic region on HCA, due to residues such as Ile91, Phe130, Val134, Leu197, Pro200, Pro201, and Leu203 (Figure 6D). The first quinoline monomer of compound **2** harbors a leucine-like side chain (Figure 1B), and the simplest arrangement places this side chain within the hydrophobic area. By employing a representation of the *P* enantiomer of **2** onto the surface of HCA, we were able to determine whether other favorable contacts could be made to support this model (Figure 6D). Another area of significant chemical shift perturbation (circle 3 in Figure 6C) was present in a negatively charged region centered on Asp72 and included Glu69, Asp71 and Asp129 (Figure 6D, right). In the proposed model of HCA–**2**, we had favorable placement of the lysine-like side chain of monomer 3 within this acidic patch. The hydroxy side chain in monomer 2 would thus coincide with the perturbation of amide residues within the last major region of chemical shift perturbation (circle 2, Figure 6C). Monomer 4 and 5 of compound **2** were located in the second turn of the foldamer helix and, therefore, were more distal to the protein surface. Nevertheless, each of these acidic side chains were located beside complementary clusters of basic residues (Figure 6D), and there were at least a few residues with notable $\Delta\delta_{H,N}$ values in the area of monomer 4 (Figure 6C).

It is therefore reasonable that the observed *P* enantiomer and regions of chemical shift perturbation both support an orientation with favorable protein–foldamer contacts. Due to the similarity between compounds **1** and **2**, it is possible that the handedness induction of HCA–**1** in solution, especially in the monomeric form when dilute, may derive from similar protein–HCA contacts. Indeed, there are similarities between the pattern of chemical shift perturbation from the analysis of HCA–**1** in Tris (Figure 2G) and that of HCA–**2** (Figure 6C). Nevertheless, significant dynamics within the complex must exist in order to facilitate the monomer–dimer transition for HCA–**1**. Dynamics within the (HCA–**1**)$_2$ dimer were suggested by the broad elution peak in size-exclusion chromatography (Figure 4B). The discrepancy between the HCA–foldamer and HCA–HCA contacts in solution (Figure 2G) and in the crystal (Figure 2H) may therefore result from a stabilization of one selected structure in the crystal from the range of possible arrangements present in solution. Additional contacts with Zn^{2+} atoms in the crystal may be one of the stabilizing constraints. Indeed, these have been shown to bridge each foldamer to an HCA molecule within (HCA–**1**)$_2$ and also to directly bridge the two HCA molecules of (HCA–**1**)$_2$, thus considerably restricting dynamics, as observed in solution in the absence of Zn^{2+}.

Finally, we noted an intriguing time-dependent evolution of several amide crosspeaks in ^{1}H,^{15}N TROSY and HSQC during NMR spectroscopy analysis of newly prepared samples of [^{15}N]HCA-**2**. Spectra acquired immediately following the addition of compound **2** to [^{15}N]HCA revealed the splitting of amide crosspeaks such as Gly6, Gly25, Glu26, Arg27, Gln28, Asn62, Gly63, Asp72, Gln74, Ile91, Lys126, Tyr127, Glu204, and Arg245. After several days, there was a complete shift towards a single set of peaks. Our hypothesis was that the initial peak doubling was due to the starting racemic state of the quinoline oligoamide portion of compound **2**, with these amide crosspeaks differentially sensitive to the *M* or *P* helices. Over time, the enantiomer preference for the *P* helix was reflected by a loss of the *M*-helix-specific crosspeak. To support this hypothesis, we prepared a fresh sample of HCA–**2** in Tris and divided the sample for simultaneous measurement by CD and NMR spectroscopy. We found by CD spectroscopy that helix handedness formed with a half-life of 9.1 h and was nearly complete (~95%) by 96 h (Figure 7). The NMR spectra mirrored

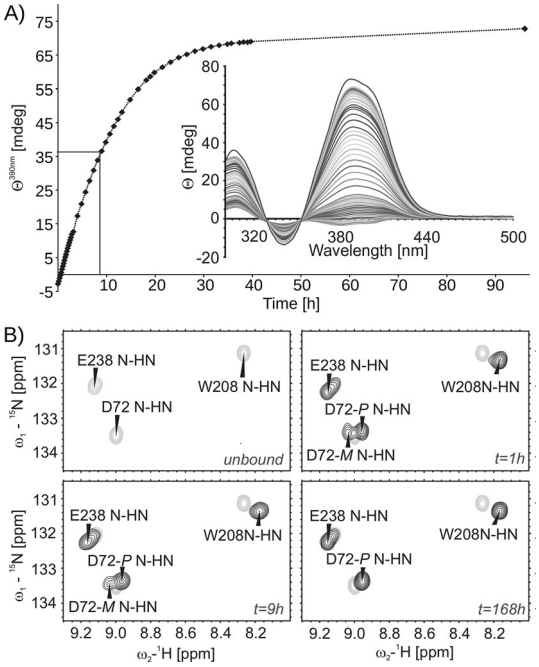

Figure 7. Kinetics of enantiomer selection in HCA–**2**, as followed by CD and NMR spectroscopy. A) Time series of θ^{390} at 293 K for freshly prepared 300 μM [^{15}N]HCA–**2** in Tris. Wavelength scans for the time series are shown in the insert. B) Region of ^{1}H,^{15}N TROSY at 293 K for unbound [^{15}N]HCA (top left), freshly prepared complex with compound **2** (top right), after 9 h (bottom left), and after several days (bottom right). The amide for Trp208 is adjacent to the sulfonamide moiety and confirms complete formation of the complex. The two peaks for Asp72 correspond to the *M* and *P* enantiomers of compound **2**.

this rate, with a difference in crosspeak intensities for spectra collected at 1, 9, and 168 h (Figure 7B). The early spectra showed approximately equal populations of the two states, which were further shifted at 9 h. A spectrum collected after several days (168 h) confirmed a complete shift to a single state. It was noted that the binding of compound **2** was al-

ready complete prior to acquisition of the first spectrum, as evidenced by the complete shift of amides surrounding the sulfonamide moiety (such as Trp 208 in Figure 7B).

The similar rates observed for handedness induction and disappearance of the doubled amide crosspeaks support the idea that the NMR spectra illustrate regions of the protein important for enantiomer stabilization and thus for foldamer–protein-selective interactions. It was noted that Asp72 is located within the acidic patch proposed to interact with the basic side chain of monomer 3 (Figure 6D). This region is a reasonable site of discrimination between the *P* and *M* enantiomers of the foldamer. The *M* helix would most likely retain hydrophobic contacts with monomer, but this would reverse the positions of monomers 3 and 4 such that charge repulsion would exist between the acidic side chain of monomer 4 and the acidic patch around Asp72.

Conclusions

Characterization of the HCA–foldamer complex in solution revealed increased dynamics but an overall similarity to the crystal structure description. Specifically, we confirmed the ability of a quinoline oligoamide foldamer to induce HCA dimerization in solution when appended to a tightly binding aromatic sulfonamide ligand. However, the dimer affinity was buffer-dependent, with a shift to a weaker dimer in Tris versus phosphate. The addition of a quinoline with an acidic side chain to the C terminus of the foldamer completely blocked dimerization. This monomeric protein–foldamer complex confirmed the ability of HCA to induce *P* helix handedness in the absence of foldamer dimerization. Surface regions on HCA comprising hydrophobic, acidic, and basic properties are suggested as the basis of enantiomeric selection, independent of Zn^{2+}. These regions were shown to contact the foldamer, based on NMR spectra comparing amide chemical shifts in the unbound and bound HCA. Although the high-resolution crystal structure provides key insights into the interaction between the foldamer and HCA, the preservation of dynamics and an ensemble of structures in solution is important for the strategic design of foldamers intended for biological applications.

Experimental Section

Synthesis: Compounds **1** and **3** were prepared as previously described.[14] Compound **2** was prepared using previously reported methods.[3c,14] The product was purified through reversed-phase (C18 column) HPLC purification; gradient: 5–100% solvent B in 30 min (Figure S7A); purified yield = 62%. Its structure and purity were assessed by 300 MHz ^{1}H NMR spectroscopy (Figure S8; chemical shifts are calibrated against the residual solvent signal of [D$_6$]DMSO [$\delta = 2.50$]), by high-resolution electrospray ionization mass spectrometry (HR-ESI-MS), and by reversed-phase HPLC. ^{1}H NMR (300 MHz, [D$_6$]DMSO/1%TFA): $\delta = 11.72$ (s, NH), 11.67 (s, NH), 11.53 (s, NH), 9.12 (t, $J = 5.9$ Hz, NH), 8.49 (dd, $J = 11.8$, 7.7 Hz, 1H), 8.23 (s, NH), 8.03–7.84 (m, 17H), 7.84–7.56 (m, 7H), 7.45–7.07 (m, 5H), 6.88–6.63 (m, 2H), 6.40 (s, 1H), 6.22 (s, 1H), 5.07–4.66 (m, 4H), 4.45–4.30 (m, 4H), 4.25–4.11 (m, 2H), 3.75 (t, $J = 6.2$ Hz, 2H), 3.29–3.11 (m, 2H), 2.76–2.58 (m, 2H), 2.46–2.20 (m, 4H), 1.48–1.36 (m, 2H), 1.32–1.12 ppm (m, 8H); HRMS: (ESI$^-$) *m/z* calcd for $[C_{80}H_{71}N_{14}O_{20}S]^-$ 1579.4695; found 1579.4753 (Figure S7B).

Protein expression and purification: Production of HCA was performed as previously reported.[30] Briefly, a pETIld vector containing wild-type human HCA was transformed into *E. coli* BL21(DE3)pLysS. Protein expression was induced by the addition of isopropyl β-D-1-thiogalactopyranoside (0.6 mM) at a culture $OD_{600\,nm}$ of 0.5, followed by growth at 37 °C for 3–5 h in the presence of $ZnSO_4$ (0.6 mM). Bacteria were collected by centrifugation and resuspended in Tris·H_2SO_4 (50 mM, pH 8.0), 0.1% Triton X-100, and benzamidine (1 mM) prior to cell lysis. After clearing the lysate by centrifugation, the supernatant was incubated for 90 min at 4 °C with affinity resin (2 mL) containing *p*-aminomethylbenzene-sulfonamide.[31] The column was washed with lysis buffer (100 mL), followed by elution of HCA with sodium acetate (25 mL, 0.1 M, pH 5.6) and sodium perchlorate (0.5 M). HCA was then dialyzed against Tris·H_2SO_4 (50 mM, pH 8.0) to remove the inhibitor and concentrated by a centrifugation filter. Isotopically enriched protein was produced by growing the bacteria in minimal M9 medium supplemented with [^{15}N]NH_4Cl (1 g L^{-1}) for ^{15}N-labeled HCA and with [^{13}C]-D-glucose (2 g L^{-1}) for ^{13}C,^{15}N-labeled HCA.

NMR spectroscopy: Samples were prepared in either sodium phosphate (50 mM, pH 7.4) or deuterated Tris (50 mM, pH 8.0), with 10% D_2O added for the lock. Complexes were formed by the addition of compound **1**, **2**, or **3** (10 mM) dissolved in DMSO. NMR experiments were conducted at a temperature of 298 or 293 K on a triple resonance Bruker Avance 700 MHz spectrometer or a cryoprobe-equipped Bruker Avance 800 MHz spectrometer. For ^{1}H,^{15}N heteronuclear 2D spectra, samples in Tris were measured by ^{1}H,^{15}N TROSY spectra at 800 MHz using a cryoprobe, whereas optimal spectra for samples in phosphate used ^{1}H,^{15}N HSQC spectra at 700 MHz. Spectra were processed by using NMRPipe/Draw[32] and analyzed by using Sparky 3 (T. D. Goddard and D. G. Kneller, University of California, San Francisco, USA). Sweep widths for recorded 3D HNCA were 12019 (^{1}H) ×2500 (^{15}N) ×5640 (^{13}C) Hz at 700 MHz and 11160 (^{1}H) ×2000 (^{15}N) ×6450 (^{13}C) Hz at 800 Mhz. Sweep widths for recorded 3D HNCO spectra were 12019 (^{1}H) ×2500 (^{15}N) ×3888 (^{13}C) Hz at 700 MHz and 11160 (^{1}H) ×2000 (^{15}N) ×6451 (^{13}C) Hz at 800 MHz. Both ^{1}H,^{15}N HSQC and ^{1}H,^{15}N TROSY spectra were used with selective 90 gauss water flip-back pulses and were recorded with sweep widths of 18028 (^{1}H) ×3333 (^{15}N) Hz or 14077 (^{15}N) ×2500 (^{15}N) Hz at 800 MHz or 700 MHz, respectively, with 2–32 scans per fid, depending on sample concentration.

Relaxation measurement: Amide ^{15}N relaxation data were measured at 700 MHz and 295 K according to a previously described method.[23] Steady-state heteronuclear {^{1}H}^{15}N NOE spectra were collected with and without 3 s of ^{1}H saturation. Relaxation rates and error calculations were determined using NMRViewJ (One Moon Scientific, New Jersey, USA).[33] Amide proton T_2 values were measured at 700 MHz and 295 K by a series of jump–return spin echo experiments[27] with delays (d_4) of 1, 2, 4, 6, and 8 ms, repeated at least two times. TopSpin 2.1 was used to determine the spectra intensity ratio (I_A/I_B), obtained for each comparison of two different delays. Amide proton T_2 relaxation rates were then calculated as described,[28] using equation $T_2 = 2\Delta d_4 \times \ln(I_A/I_B)^{-1}$ for each possible combination of Δd_4 and I_A/I_B. The values of $^1H^N$ T_2 were calculated as the average value of each delay comparison, with the error value equal to the standard deviation. Correlation times (τ_C) were calculated from the equation $\tau_C = (T_2 k)$, where k is approximately equal to five but can be indirectly determined for a sample series at a given temperature and field strength.

Circular dichroism: CD spectra were recorded on a Jasco J-815 Circular Dichroism spectrometer using quartz cells of 1, 2, or 5 mm optical path length. Scans were measured at 20 °C over a wavelength range of 300–500 nm, with a response time of 0.5 s and a scanning speed of 50 nm min^{-1}. All CD spectra were baseline-corrected for signal contributions due to the buffer containing HCA (using solutions with matching concentrations of HCA with 2% DMSO in sodium phosphate buffer (50 mM, pH 7.4) or in Tris (50 mM, pH 8.0). Samples were prepared by adding 1 equiv of the foldamer (dissolved in DMSO at a concentration of 10 mM) to a solution containing HCA in sodium phosphate (50 mM, pH 7.4) or Tris (50 mM, pH 8.0). CD experiments were carried out to follow the interaction of the foldamers with the protein and helix handedness preference as a function of time or concentration. For the kinetic study, CD spectra were recorded starting immediately after the addition of the foldamer to the protein over 96 h (one scan per spectrum). For the concentration study, samples with different protein concentrations, each containing 1 equiv of foldamer, were incubated for sufficient time to reach equilibrium (24 h for the HCA–**1** complex, 48 h for HCA–**2** in phosphate, and 92 h for HCA–**2** in Tris). CD spectra were obtained as an average of 2–6 scans, depending on concentration. Protein concentrations were calculated based on UV/Vis spectroscopy (Eppendorf Biophotometer Plus) at 280 nm with an extinction coefficient (ε^{280}) of 50 420 M^{-1} cm^{-1}. Foldamer concentrations were determined by UV/Vis spectroscopy (NanoDrop ND-1000) at 325 nm with ε^{280} values of 2676.8 M^{-1} cm^{-1} for **1** and 3346 M^{-1} cm^{-1} for **2**.

Size-exclusion chromatography: Samples (500 μL) of HCA, HCA–**1** or HCA–**2** (500 μM) in phosphate buffer (pH 7.4) were analyzed by using a Superdex 75 10/300 GL column (GE Healthcare Life Sciences) using phosphate buffer (pH 7.4) with a flow rate of 0.4 mL min^{-1} and detection at 280 nm.

Acknowledgements

Assignment of HCA was aided by the list of backbone chemical shifts provided by Ronald Venters. We thank Sabrina Rousseau and Thierry Dakhli for assistance with production of HCA. We also thank Axelle Grélard, Estelle Morvan, and the structural biology platform at the Institut Européen de Chimie et Biologie (UMS 3033) for access to NMR spectrometers, equipment, and technical assistance. Financial support from the Centre Nationale de la Recherche Scientifique (IR-RMN-THC Fr3050) is gratefully acknowledged. M.J. is funded by the Polish Ministry of Science and Higher Education (Mobility Plus Program), and C.C. was supported by a post-doctoral fellowship from European Union grant FP7-IAPP-2008-230662-Foldappi.

Keywords: circular dichroism · foldamers · human carbonic anhydrase · molecular recognition · nuclear magnetic resonance

[1] C. M. Goodman, S. Choi, S. Shandler, W. F. DeGrado, *Nat. Chem. Biol.* **2007**, *3*, 252 – 262; G. Guichard, I. Huc, *Chem. Commun.* **2011**, *47*, 5933 – 5941.

[2] For reviews: I. Huc, *Eur. J. Org. Chem.* **2004**, 17 – 29; D.-W. Zhang, X. Zhao, J.-L. Hou, Z.-T. Li, *Chem. Rev.* **2012**, *112*, 5271 – 5316.

[3] a) N. R. Wurtz, J. M. Turner, E. E. Baird, P. B. Dervan, *Org. Lett.* **2001**, *3*, 1201 – 1203; b) H. M. König, R. Abbel, D. Schollmeyer, A. F. M. Kilbinger, *Org. Lett.* **2006**, *8*, 1819 – 1822; c) B. Baptiste, C. Douat-Casassus, K. Laxmi-Reddy, F. Godde, I. Huc, *J. Org. Chem.* **2010**, *75*, 7175 – 7185; d) N. S. Murphy, P. Prabhakaran, V. Azzarito, J. P. Plante, M. J. Hardie, C. A. Kilner, S. L. Warriner, A. J. Wilson, *Chem. Eur. J.* **2013**, *19*, 5546 – 5550.

[4] N. Delsuc, J.-M. Léger, S. Massip, I. Huc, *Angew. Chem. Int. Ed.* **2007**, *46*, 214 – 217; *Angew. Chem.* **2007**, *119*, 218 – 221; N. Delsuc, S. Massip, J.-M. Léger, B. Kauffmann, I. Huc, *J. Am. Chem. Soc.* **2011**, *133*, 3165 – 3172.

[5] a) J. T. Ernst, J. Becerril, H. S. Park, H. Yin, A. D. Hamilton, *Angew. Chem. Int. Ed.* **2003**, *42*, 535 – 539; *Angew. Chem.* **2003**, *115*, 553 – 557; b) E. R. Gillies, F. Deiss, C. Staedel, J.-M. Schmitter, I. Huc, *Angew. Chem. Int. Ed.* **2007**, *46*, 4081 – 4084; *Angew. Chem.* **2007**, *119*, 4159 – 4162.

[6] T. Qi, V. Maurizot, H. Noguchi, T. Charoenraks, B. Kauffmann, M. Takafuji, H. Ihara, I. Huc, *Chem. Commun.* **2012**, *48*, 6337 – 6339.

[7] E. F. Lee, J. D. Sadowsky, B. J. Smith, P. E. Czabotar, K. J. Peterson-Kaufman, P. M. Colman, S. H. Gellman, W. D. Fairlie, *Angew. Chem. Int. Ed.* **2009**, *48*, 4318 – 4322; *Angew. Chem.* **2009**, *121*, 4382 – 4386; W. S. Horne, L. M. Johnson, T. J. Ketas, P. J. Klasse, M. Lu, J. P. Moore, S. H. Gellman, *Proc. Natl. Acad. Sci. USA* **2009**, *106*, 14751 – 14756; E. A. Harker, A. Schepartz, *ChemBioChem* **2009**, *10*, 990 – 993; M. D. Boersma, H. S. Haase, K. J. Peterson-Kaufman, E. F. Lee, O. B. Clarke, P. M. Colman, B. J. Smith, W. S. Horne, W. D. Fairlie, S. H. Gellman, *J. Am. Chem. Soc.* **2012**, *134*, 315 – 323; L. M. Johnson, S. Barrick, M. V. Hager, A. McFedries, E. A. Homan, M. E. Rabaglia, M. P. Keller, A. D. Attie, A. Saghatelian, A. Bisello, S. H. Gellman, *J. Am. Chem. Soc.* **2014**, *136*, 12848 – 12851; J. W. Checco, D. F. Kreitler, N. C. Thomas, D. G. Belair, N. J. Rettko, W. L. Murphy, K. T. Forest, S. H. Gellman, *Proc. Natl. Acad. Sci. USA* **2015**, *112*, 4552 – 4557.

[8] B. P. Orner, J. T. Ernst, A. D. Hamilton, *J. Am. Chem. Soc.* **2001**, *123*, 5382 – 5383; J. P. Plante, T. Burnley, B. Malkova, M. E. Webb, S. L. Warriner, T. A. Edwards, A. J. Wilson, *Chem. Commun.* **2009**, 5091 – 5093; F. Campbell, J. P. Plante, T. A. Edwards, S. L. Warriner, A. J. Wilson, *Org. Biomol. Chem.* **2010**, *8*, 2344 – 2351; V. Azzarito, P. Prabhakaran, A. I. Bartlett, N. S. Murphy, M. J. Hardie, C. A. Kilner, T. A. Edwards, S. L. Warriner, A. J. Wilson, *Org. Biomol. Chem.* **2012**, *10*, 6469 – 6472; G. M. Burslem, H. F. Kyle, A. L. Breeze, T. A. Edwards, A. Nelson, S. L. Warriner, A. J. Wilson, *ChemBioChem* **2014**, *15*, 1083 – 1087; A. Barnard, K. Long, H. L. Martin, J. A. Miles, T. A. Edwards, D. C. Tomlinson, A. Macdonald, A. J. Wilson, *Angew. Chem. Int. Ed.* **2015**, *54*, 2960 – 2965; *Angew. Chem.* **2015**, *127*, 3003 – 3008; V. Azzarito, J. A. Miles, J. Fisher, T. A. Edwards, S. L. Warriner, A. J. Wilson, *Chem. Sci.* **2015**, *6*, 2434 – 2443; J. M. Rodriguez, A. D. Hamilton, *Angew. Chem. Int. Ed.* **2007**, *46*, 8614 – 8617; *Angew. Chem.* **2007**, *119*, 8768 – 8771; J. M. Rodriguez, N. T. Ross, W. P. Katt, D. Dhar, G. Lee, A. D. Hamilton, *ChemMedChem* **2009**, *4*, 649 – 656; O. V. Kulikov, A. D. Hamilton, *RSC Adv.* **2012**, *2*, 2454 – 2461; W. E. Martucci, J. M. Rodriguez, M. A. Vargo, M. Marr, A. D. Hamilton, K. S. Anderson, *Med. Chem. Commun.* **2013**, *4*, 1247 – 1256; O. V. Kulikov, S. Kumar, M. Magzoub, P. C. Knipe, I. Saraogi, S. Thompson, A. D. Miranker, A. D. Hamilton, *Tetrahedron Lett.* **2015**, *56*, 3670 – 3673; O. Kutzki, H. S. Park, J. T. Ernst, B. P. Orner, H. Yin, A. D. Hamilton, *J. Am. Chem. Soc.* **2002**, *124*, 11838 – 11839; H. Yin, G. Lee, K. A. Sedey, O. Kutzki, H. S. Park, B. P. Orner, J. T. Ernst, H.-G. Wang, S. M. Sebti, A. D. Hamilton, *J. Am. Chem. Soc.* **2005**, *127*, 10191 – 10196; H. Yin, G. Lee, H. S. Park, G. A. Payne, J. M. Rodriguez, S. M. Sebti, A. D. Hamilton, *Angew. Chem. Int. Ed.* **2005**, *44*, 2704 – 2707; *Angew. Chem.* **2005**, *117*, 2764 – 2767; S. M. Biros, L. Moisan, E. Mann, A. Carella, D. Zhai, J. C. Reed, J. Rebek, Jr., *Bioorg. Med. Chem. Lett.* **2007**, *17*, 4641 – 4645; C. G. Cummings, N. T. Ross, W. P. Katt, A. D. Hamilton, *Org. Lett.* **2009**, *11*, 25 – 28; A. Kazi, J. Sun, K. Doi, S.-S. Sung, Y. Takahashi, H. Yin, J. M. Rodriguez, J. Becerril, N. Berndt, A. D. Hamilton, H.-G. Wang, S. M. Sebti, *J. Biol. Chem.* **2011**, *286*, 9382 – 9392; A. Raghuraman, E. Ko, L. M. Perez, T. R. Ioerger, K. Burgess, *J. Am. Chem. Soc.* **2011**, *133*, 12350 – 12353; A. S. Voisin-Chiret, G. Burzicki, S. Perato, M. De Giorgi, C. Franchini, J. S.-d. O. Santos, S. Rault, *Tetrahedron* **2012**, *68*, 4381 – 4389; D. Xin, E. Ko, L. M. Perez, T. R. Loerger, K. Burgess, *Org. Biomol. Chem.* **2013**, *11*, 7789 – 7801; D. Xin, L. M. Perez, T. R. Loerger, K. Burgess, *Angew. Chem. Int. Ed.* **2014**, *53*, 3594 – 3598; *Angew. Chem.* **2014**, *126*, 3668 – 3672; C. Gloaguen, A. S. Voisin-Chiret, J. S.-d. O. Santos, J. Fogha, F. Gautier, M. De Giorgi, G. Burzicki, S. Perato, C. Pétigny-Lechartier, K. S.-L. Jeune, E. Brotin, D. Goux, M. N'Diaye, B. Lambert, M.-H. Louis, L. Ligat, F. Lopez, P. Juin, R. Bureau, S. Rault, L. Poulain, *J. Med. Chem.* **2015**, *58*, 1644 – 1668.

[9] J. A. Hebda, I. Saraogi, M. Magzoub, A. D. Hamilton, A. D. Miranker, *Chem. Biol.* **2009**, *16*, 943 – 950; I. Saraogi, J. A. Hebda, J. Becerril, L. A. Estroff, A. D. Miranker, A. D. Hamilton, *Angew. Chem. Int. Ed.* **2010**, *49*,

736 – 739; *Angew. Chem.* **2010**, *122*, 748 – 751; S. Kumar, A. D. Miranker, *Chem. Commun.* **2013**, *49*, 4749 – 4751; S. Kumar, D. E. Schlamadinger, M. A. Brown, J. M. Dunn, B. Mercado, J. A. Hebda, I. Saraogi, E. Rhoades, A. D. Hamilton, A. D. Miranker, *Chem. Biol.* **2015**, *22*, 369 – 378.

[10] P. B. Dervan, B. S. Edelson, *Curr. Opin. Struct. Biol.* **2003**, *13*, 284 – 299; T. Bando, H. Sugiyama, *Acc. Chem. Res.* **2006**, *39*, 935 – 944; R. D. Taylor, Y. Kawamoto, K. Hashiya, T. Bando, H. Sugiyama, *Chem. Asian J.* **2014**, *9*, 2527 – 2533.

[11] a) P. S. Shirude, E. R. Gillies, S. Ladame, F. Godde, K. Shin-ya, I. Huc, S. Balasubramanian, *J. Am. Chem. Soc.* **2007**, *129*, 11890 – 11891; b) L. Delaurière, Z. Dong, K. Laxmi-Reddy, F. Godde, J.-J. Toulmé, I. Huc, *Angew. Chem. Int. Ed.* **2012**, *51*, 473 – 477; *Angew. Chem.* **2012**, *124*, 488 – 492; c) S. Müller, K. Laxmi-Reddy, P. V. Jena, B. Baptiste, Z. Dong, F. Godde, T. Ha, R. Rodriguez, S. Balasubramanian, I. Huc, *ChemBioChem* **2014**, *15*, 2563 – 2570.

[12] N. Chandramouli, Y. Ferrand, G. Lautrette, B. Kauffmann, C. D. Mackereth, M. Laguerre, D. Dubreuil, I. Huc, *Nat. Chem.* **2015**, *7*, 334 – 341.

[13] For a crystal structure, see: C. L. Kielkopf, S. White, J. W. Szewczyk, J. M. Turner, E. E. Baird, P. B. Dervan, D. C. Rees, *Science* **1998**, *282*, 111 – 115. For solution studies, see: R. P. L. de Clairac, B. H. Geierstanger, M. Mrksich, P. B. Dervan, D. E. Wemmer, *J. Am. Chem. Soc.* **1997**, *119*, 7909 – 7916; C. A. Hawkins, R. P. de Clairac, R. N. Dominey, E. E. Baird, S. White, P. B. Dervan, D. E. Wemmer, *J. Am. Chem. Soc.* **2000**, *122*, 5235 – 5243.

[14] J. Buratto, C. Colombo, M. Stupfel, S. J. Dawson, C. Dolain, B. L. d'Estaintot, L. Fischer, T. Granier, M. Laguerre, B. Gallois, I. Huc, *Angew. Chem. Int. Ed.* **2014**, *53*, 883 – 887; *Angew. Chem.* **2014**, *126*, 902 – 906.

[15] For other examples of HCA surface binding exploration assisted by a tethered ligand, see: a) A. Jain, S. G. Huang, G. M. Whitesides, *J. Am. Chem. Soc.* **1994**, *116*, 5057; b) A. Jain, G. M. Whitesides, R. S. Alexander, D. W. Christianson, *J. Med. Chem.* **1994**, *37*, 2100; c) T. Andersson, M. Lundquist, G. T. Dolphin, K. Enander, B.-H. Jonsson, J. W. Nilsson, L. Baltzer, *Chem. Biol.* **2005**, *12*, 1245; d) L. T. Tegler, K. Fromell, B.-H. Jonsson, J. Viljanen, C. Winander, J. Carlsson, L. Baltzer, *ChemBioChem* **2011**, *12*, 559; e) K. Enander, G. T. Dolphin, L. Baltzer, *J. Am. Chem. Soc.* **2004**, *126*, 4464; f) A. L. Banerjee, M. Swanson, B. C. Roy, X. Jia, M. K. Haldar, S. Mallik, D. K. Srivastava, *J. Am. Chem. Soc.* **2004**, *126*, 10875.

[16] Such handedness induction has also been evidenced upon binding to DNA (ref. [11a]), to saccharides (ref. [12]), or upon attaching a chiral copula: A. M. Kendhale, L. Poniman, Z. Dong, K. Laxmi-Reddy, B. Kauffmann, Y. Ferrand, I. Huc, *J. Org. Chem.* **2011**, *76*, 195 – 200; S. J. Dawson, Á. Mészáros, L. Pethő, C. Colombo, M. Csékei, A. Kotschy, I. Huc, *Eur. J. Org. Chem.* **2014**, 4265 – 4275.

[17] For another example of a protein-induced handedness induction in a helical molecule, see: H. Onouchi, T. Hasegawa, D. Kashiwagi, H. Ishiguro, K. Maeda, E. Yashima, *J. Polym. Sci. Part A* **2006**, *44*, 5039 – 5048.

[18] A. M. Watkins, M. G. Wuo, P. S. Arora, *J. Am. Chem. Soc.* **2015**, *137*, 11622 – 11630.

[19] S. J. Kopytek, R. F. Standaert, J. C. Dyer, J. C. Hu, *Chem. Biol.* **2000**, *7*, 313 – 321; C. T. Rollins, V. M. Rivera, D. N. Woolfson, T. Keenan, M. Hatada, S. E. Adams, L. J. Andrade, D. Yaeger, M. R. van Schravendijk, D. A. Holt, M. Gilman, T. Clackson, *Proc. Natl. Acad. Sci. USA* **2000**, *97*, 7096 – 7101; A. Fegan, B. White, J. C. T. Carlson, C. R. Wagner, *Chem. Rev.* **2010**, *110*, 3315 – 3336; D. Erhart, M. Zimmermann, O. Jacques, M. B. Wittwer, B. Ernst, E. Constable, M. Zvelebil, F. Beaufils, M. P. Wymann, *Chem. Biol.* **2013**, *20*, 549 – 557; A. Barnard, J. A. Miles, G. M. Burslem, A. M. Barker, A. J. Wilson, *Org. Biomol. Chem.* **2015**, *13*, 258 – 264.

[20] For a related study, see ref. [15c].

[21] R. A. Venters, B. T. Farmer II, C. A. Fierke, L. D. Spicer, *J. Mol. Biol.* **1996**, *264*, 1101 – 1116.

[22] M. P. Williamson, *Prog. NMR Spectrosc.* **2013**, *73*, 1 – 16.

[23] N. A. Farrow, R. Muhandiram, A. U. Singer, S. M. Pascal, C. M. Kay, G. Gish, S. E. Shoelson, T. Pawson, J. D. Forman-Kay, L. E. Kay, *Biochemistry* **1994**, *33*, 5984 – 6003.

[24] J. García de La Torre, M. L. Huertas, B. Carrasco, *J. Magn. Reson.* **2000**, *147*, 138 – 146.

[25] A. E. Eriksson, T. A. Jones, A. Liljas, *Proteins Struct. Funct. Genet.* **1988**, *4*, 274 – 282.

[26] P. Dosset, J.-C. Hus, M. Blackledge, D. Marion, *J. Biomol. NMR* **2000**, *16*, 23 – 28.

[27] V. Sklenář, A. Bax, *J. Magn. Reson.* **1987**, *74*, 469 – 479.

[28] J. Anglister, S. Grzesiek, H. Ren, C. B. Klee, A. Bax, *J. Biomol. NMR* **1993**, *3*, 121 – 126.

[29] N. Delsuc, T. Kawanami, J. Lefeuvre, A. Shundo, H. Ihara, M. Takafuji, I. Huc, *ChemPhysChem* **2008**, *9*, 1882 – 1890.

[30] P. Y. Hu, A. Waheed, W. S. Sly, *Proc. Natl. Acad. Sci. USA* **1995**, *92*, 2136 – 2140.

[31] X. L. Zhu, W. S. Sly, *J. Biol. Chem.* **1990**, *265*, 8795 – 8801.

[32] F. Delaglio, S. Grzesiek, G. W. Vuister, G. Zhu, J. Pfeifer, A. Bax, *J. Biomol. NMR* **1995**, *6*, 277 – 293.

[33] B. A. Johnson, *Methods Mol. Biol.* **2004**, *278*, 313 – 352.

Manuscript received: November 17, 2015

Accepted article published: January 25, 2016

Final article published: March 4, 2016